Hybrid Drainage Technique application on bimodal limestone

Victor Fernandes[1,3,*], *Franck* Nono[2], *Benjamin* Nicot[1], *Fabrice* Pairoys[1], *Henri* Bertin[3], *Jean* Lachaud[3] and *Cyril* Caubit[1]

[1]TotalEnergies, CSTJF, Avenue Larribau, 64000 Pau, France
[2]Akkodis, 4 Rue Jules Ferry, 64000 Pau, France
[3]I2M-Université de Bordeaux, CNRS, 351, Cours de la Libération, 33405 Talence, France

Abstract. Representative relative permeability and capillary pressure must be provided for reliable reservoir production forecasts. These petrophysical parameters are mostly obtained through laboratory experimental work and numerical simulation. Thus, appropriate techniques are necessary for restoring initial water saturation and wettability. In a previous paper [1], we presented the Hybrid Drainage Technique (HDT), which is a primary drainage method used in water/oil systems. It generates homogeneous water saturation profile at targeted S_{wi} value in reduced experimental duration compared to the Porous Plate method. The proof-of-concept study was successfully applied to simple rocks, such as Bentheimer and Richemont outcrop samples. In this paper, we tested a more complex bimodal system, represented by the Estaillades limestone rock, with the aim of comparing the HDT with the Viscous Oil Flood method (VOF). Primary drainage by VOF is commonly used on full-size cores, as it is very time consuming to desaturate large rocks to S_{wi} by the Porous Plate method and impossible to use the centrifuge technique. The points of interest for this comparison are as follows: reaching the targeted S_{wi} value, homogeneity of the saturation profile at the end of primary drainage, wettability alteration and imbibition interpretation via history-matching process of differential pressure, oil production and saturation profiles when available. During VOF experiments, we noticed a difficulty in obtaining low values of S_{wi} (below 35%). This could be due to the dual-porosity nature of the Estaillades limestone and the poor connectivity between large and small pore networks. On the other hand, the capillary-pressure controlled step of the HDT provides access to both porosity networks, thus reaching lower S_{wi} values. Furthermore, the invasion process is different for the two techniques. Therefore, even if the same S_{wi} value is obtained, pore occupancy at the end of primary drainage is different on such bimodal pore network. This will also impact wettability alteration, thus imbibition results. Monitoring using both NMR and Micro-Tomography imaging allowed visualization of fluid saturation and distribution at pore and core scales. These were not only valuable input data for interpreting flooding experiments through numerical simulations, but also for phenomenological understanding.

1 Background and state of the art

In order to study and evaluate the potential production of a petroleum reservoir, numerical simulations are performed. The inputs for the numerical simulations are mainly the relative permeability (K_r) and the capillary pressure (P_c) curves during water injection, in the case of a water/oil experiment. These data are still mostly obtained from laboratory experiments performing Special Core Analysis (SCAL) studies, which reproduce several stages that the reservoir undergoes during its exploitation, though efforts to estimate those properties in situ are on-going with different challenges and difficulties [2 - 4].

This paper focuses on the restored state method, that consists of coring a rock sample from a reservoir well with objective driven coring fluid [5], sampling and plugging in the appropriate dimensions (usually cylindrical samples, varying from 1" and 1.5" in diameter and up to 3" in length [6]. The initial step of a conventional procedure for reproduction of reservoir conditions consists in taking the sample to its initial state in terms of wettability. For that matter, the sample is cleaned with the objective of removing native oil, mud filtrates, precipitated salts and connate water. In this process, water, CO_2 and a variety of organic non-polar and polar solvents may be used to ensure appropriate cleaning intended to produce a water-wet sample, a nontrivial process [7]. The sample is then submitted to conventional or vacuum oven-drying as well as flow through drying (by using, for instance, N_2).

The following step consists in setting fluids initial saturation, in a process called primary drainage (PD). In the case of an oil/water system, this phase consists of injecting oil in a water-saturated sample. This phase mimics the migration phase of hydrocarbons from the source rock to the reservoir [8]. After reaching the target value of initial water saturation (S_{wi}), which is defined by the response of the reservoir logging relative to the region where the sample was cored, a wettability restoration phase is performed by ageing the core sample in its own crude oil at reservoir temperature and pore pressure, which prevent water loss. After these steps, the sample may be considered as restored to its original state of wettability and fluid settings.

In order to experimentally simulate the reservoir behaviour during hydrocarbon production, brine injection in the core at the S_{wi} state follows the ageing step. This stage is called the imbibition (waterflooding), that will take the sample from an S_{wi} to a Remaining Oil Saturation (ROS)

* Corresponding author: victor.de-oliveira-fernandes@totalenergies.com

state (ROS vs Sor, [9]). During this phase, the oil production rate, the saturation profile dynamics, and the pressure drop across the sample allow the determination of K_r and P_c by inverse analysis. However, any error committed when setting fluids initial saturation and restoring rock's wettability will impact the sample response during imbibition, leading to uncertainties on K_r and P_c estimations.

Therefore, this paper establishes the following two objectives to investigate the initial fluid setting on bimodal limestone rocks:

i. To present the difficulty to reach low target S_{wi} values during oil/water primary drainage on bimodal limestone samples using viscous-controlled techniques (*e.g.*, Viscous Oil Flood, VOF) and provide a solution to this problem (Hybrid Drainage Technique, HDT).
ii. To compare the results in terms of K_r, P_c and pore occupancy during the waterflooding of twin samples drained at the same value of S_{wi} by VOF and HDT.

In order to obtain information in both the pore and core scales during our experiments, we performed NMR and Micro-tomography (μ-CT) imaging. These are important tools to access core porosity heterogeneity, to monitor fluids behaviour during the different core floods in a SCAL protocol and to provide information regarding the rock wettability.

The possibility of using both imaging tools to monitor the same sample during the experimental cycle, thanks to the overburden cell presented in [1], provides an innovative aspect to this study.

1.1 Importance of reaching a correct and homogeneous Swi profile during primary drainage

Reaching a correct value of S_{wi} at the end of primary drainage is important because wettability alteration during ageing is dependent on the sample initial oil saturation. This evidence was analyzed by different authors on both sandstone and limestone outcrop samples [10 - 12].

Nonetheless, simply reaching a target value of S_{wi} may hide some artifacts. The main artifact impacting the establishment of a homogeneous S_{wi} profile is Capillary End Effects (CEE). These effects arise from a discontinuity in capillary forces, which tends to trap the wetting phase [13]. This generates a build-up in the wetting phase saturation close to the outlet thus reducing the non-wetting phase permeability.

CEE must be corrected before any SCAL tests as it does not represent a real behavior of fluids migration phase in the reservoir (where these effects will only be observed close to the production wells). Furthermore, a pore occupancy representative of the reservoir at the end of primary drainage must be achieved in order to represent the appropriate conditions of fluids placement in the porous medium. The achievement of this condition is even more challenging in the case of bimodal samples, where a by-passing of the smaller porosity may occur when a viscous-controlled method is adopted, such as the Viscous Oil Flood. On the other hand, a capillary-pressure controlled technique, such as the Porous Plate, is able to overcome this issue, given that a homogeneous capillary pressure field is applied on the sample.

The impact of CEE presence during wettability restoration, thus on imbibition K_r and P_c calculation, is a more complicated issue. One of the hypotheses for the inverse analysis during the history match is that the wettability of the core is homogeneous, so that K_r and P_c will have a constant behaviour along the core. However, as wettability change during ageing is dependent on fluid saturations, a non-uniform wettability profile will result from a sample for which capillary end effects have not been removed [14]. Furthermore, maintaining a homogeneous saturation profile during ageing is a necessary but insufficient condition for homogeneous wettability restoration. It has been shown that a heterogeneous wettability profile may result even when a homogeneous saturation profile is ensured during ageing, depending on the adopted ageing technique. [15 - 17].

1.2 Viscous Oil Flood and Hybrid Drainage Technique

The most widely used technique for setting initial water saturation, the Viscous Oil Flood consists in injecting oil at constant flowrate steps in an initially fully water-saturated sample, while measuring the pressure drop between inlet and outlet as well as fluid production [18]. This method may be performed either by injection of both phases (steady-state) at different flowrate ratios or by injection of only one phase (unsteady-state). In this work, we will focus on the unsteady-state technique, used on the experimental work.

Until oil breakthrough, only water will be produced as oil percolates in the sample. After oil breakthrough, a production of both phases will be observed until brine production ceases, in the unsteady-state case. This is a fast technique that does not require a particular setup, being possible to be carried out in the same cell used for the following steps of SCAL (ageing and flooding) and by a simple injection rig.

This method allows the direct measurement of end-point effective permeability from simple application of the multiphase Darcy's Law [6]. To perform the measurement of the effective permeability ($K_{eff}(S_w)$), a steady flow of both the injected and produced phase, and a constant dP must be attained. For this reason, in the case of unsteady-state experiments, the measurement of only the injected phase K_{eff} is possible, as only the injected phase may reach a steady flow.

During oil injection, there are three important data to record: pressure drop along the injection axis, water and oil production at the outlet and the saturation profiles during core flood.

The main issue about this technique is the generation of CEE during primary drainage. To avoid this situation, laboratories usually apply high flowrates to reduce Capillary-End Effects. Nonetheless, this does not represent actual flow in the reservoir. Moreover, this approach may cause irreversible damage in the core, such as fines migration and additional pore volume creation, impacting further measurements once the rock matrix has been modified.

A solution to eliminate capillary end effects is reversing the direction of oil injection. Although this method may produce a homogeneous saturation profile, two major issues may outcome:

- Unwanted imbibition from the mobilization of the brine concentrated at the sample outlet. This brine will be displaced towards the initial inlet, increasing water saturation at these points, which may complicate the oil and water distribution due to hysteresis.

- Formation of disconnected oil clusters that will adversely affect wettability restoration and impact effective permeability measurements [19].

Inspired by the challenges and the propositions made by different authors, we proposed a new Hybrid Drainage Technique (HDT) capable of not only reducing experimental time in comparison to a classic Porous Plate primary drainage, but also generating a homogeneous saturation profile [1].

The principle of HDT consists of coupling Viscous Oil Flood (Step 1) and Porous Plate (Step 2) to perform fast primary drainage, free from capillary end effects, as the final step of the method is capillary-driven and generates a homogeneous capillary pressure field in the sample.

As well as in other capillary-driven techniques (*e.g.*, Porous Plate and Centrifuge), knowing the target P_c is mandatory for reaching a correct S_{wi} value using HDT.

The main benefits of this technique are experimental time reduction and a homogenous saturation profile generation. The time reduction is due to fast water production from Viscous Oil Flood while the latter results from a very quick transition to Porous Plate drainage without sample unloading. In addition, after establishing S_{wi}, the sample is immediately ready for further testing as it always remains in the experimental cell with confining stress.

1.3 The challenge on setting low values of Swi on bimodal limestone

Given the dual-porosity aspect of some limestones, associated with a poor connectivity between small and big pores, setting the appropriate value of S_{wi} during primary drainage may be challenging. This is the case of the Estaillades limestone.

Authors have reported difficulty on setting low values of S_{wi} on these samples by both Viscous Flooding and Centrifugation [20 -23]. The poor connectivity between the pore networks was identified by different studies, which may indicate the main reason for the difficult fluid initialization in the ideal conditions of Initial Water Saturation [21, 24, 25].

2 Methodology

2.1 Solid and fluids

To test the behavior of bimodal limestone samples during primary drainage, we used the Estaillades limestone, an outcrop sample from the Burdigalian age, extracted from a stone-pit in France, and largely used in the petrophysical field due to its porosity characteristics.

A nomenclature code was established for identification of the samples and primary drainage methods used. The samples are named following the logic: XXX-YYY, where:

- XXX designates the rock type – EST for Estaillades.
- YYY designates the primary drainage method used – VOF for Viscous Oil Flood and HDT for Hybrid Drainage Technique.

We used 3 samples of the same size ($D = 38\ mm$; $L = 50\ mm$) and one mini-plug (EST-HDT-03 – $D = 10\ mm$; $L = 30\ mm$).

The dual-porosity aspect of the Estaillades samples may be clearly observed in the result of an MICP experiment presented in Fig. 1.

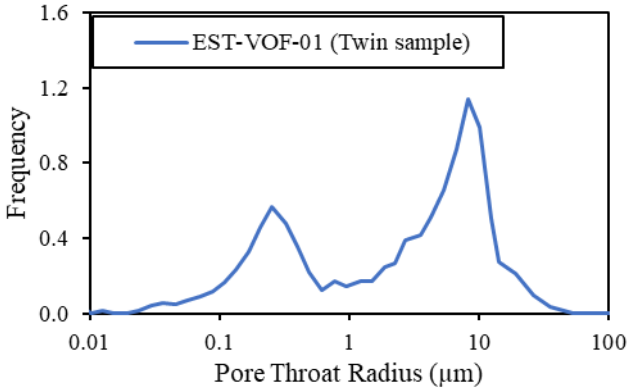

Fig. 1. Pore Throat Radius distribution from MICP (EST-VOF-01 twin sample) experiments.

The conventional petrophysical properties (Φ and K_w) of the samples used in this study are presented in Table 1.

Table 1 - CCA data for Estaillades samples used in the experiments

Sample	Vp (Φ)	Kw
EST-VOF-01	17.06 cc (30.5 %)	196 mD
EST-HDT-01	16.49 cc (28.8 %)	131 mD
EST-HDT-02	18.08 cc (31.6 %)	260 mD
EST-HDT-03	0.62 cc (28.1 %)	103 mD

In order to allow an unambiguous detection of hydrocarbon by NMR, deuterium oxide (D_2O) was used for the aqueous phase on experiments done on EST-VOF-01, EST-HDT-02 and EST-HDT-03, since this fluid is not detected by NMR acquisitions. In addition, Potassium Iodide (KI) was added to the aqueous solution to improve the X-ray Micro-tomography imaging of the samples. Marcol™ 52, a synthetic oil manufactured by ExxonMobil, was used as non-wetting phase during primary drainage and waterflooding (exclusively in the case of EST-VOF-01, FINAVESTAN A 180 B was also used during primary drainage). A dead crude oil (O1) from an African reservoir was used for ageing the core samples and altering the wettability. A toluene flush at ambient temperature was performed as a buffer after primary drainage in mineral synthetic oil and after ageing in crude oil. This step prevents a potential asphaltene precipitation when mineral and crude oil are in contact [9, 26, 27].

Basic properties of the fluids used in the experiments are presented in Table 2.

Table 2 - Basic properties of fluids used in experiments

Fluid	Composition	Density	Viscosity
Brine (B1)	D_2O + KI @ 50 g/l + $CaCl_2$ @ 20 g/l	1.15 g/cc	1.26 cP
Brine (B2)	H_2O + KI @ 50 g/l + $CaCl_2$ @ 20 g/l	1.05 g/cc	1.06 cP
Mineral Oil	Marcol™ 52	0.83 g/cc	12.00 cP
Mineral Oil	FINAVESTAN A 180 B	0.86 g//cc	63.60 cP
Dead Oil	O1	0.90 g/cc	42.44 cP
Solvent	Toluene	0.86 g/cc	0.56 cP

It is important to precise that, for performing differential imaging processing on the µ-CT images of sample EST-

HDT-03, we fully saturated it with 300 g/l of KI doped brine [28]. Furthermore, Galden® HT270 fluorinated oil from Solvay was used as confinement fluid, as it produces no NMR signal.

2.2 Experimental setup and protocol

The experimental setup used to perform both oil injections during VOF and HDT, and the waterflooding experiments is similar, between each other. The only difference is the use of the platen housing the porous plate on HDT versus a regular diffuser on VOF. During waterflooding, brine is injected by the bottom of the sample, in order to perform a gravity-stable displacement. The setup is described in detail previously [1].

The overburden cell used for the experiments is metallic-free, being entirely made in PEEK®, as well as all flow lines. This is important as this material produces no NMR signal and has reduced radiography attenuation. The porous plate used for the HDT experiments is made of porous alumina, with a typical pore radius of 90 nm.

All experiments were conducted at ambient temperature, except for the ageing step, performed at 80 °C. From the brine-saturated state up to the end of the waterflooding, samples were kept under pore pressure of 2 bars and confinement pressure of 30 bars, which leads to a Net Confining Stress of 28 bars.

The samples followed a complete restored state K_r imbibition cycle, that includes, beside the Conventional Characterization Analysis (CCA) steps, primary drainage, ageing and waterflooding.

To perform waterflooding at the same initial condition in terms of water saturation, samples EST-HDT-02 and EST-HDT-03 were initialized at the same value of S_{wi} ($S_{wi} \approx 0.38$) as EST-VOF-01, given the difficulty of the VOF technique to reach lower values. In order to prove the capacity of HDT to reach lower target S_{wi} values, sample EST-HDT-01 was initialized at $S_{wi} \approx 0.20$.

A numerical simulation was done to obtain interpreted K_r and P_c imbibition curves from the history match of the pressure drop, oil production and water saturation profiles of samples EST-VOF-01 and EST-HDT-02. These were the selected samples for comparison of VOF and HDT techniques.

2.3 Imaging acquisition and processing

The NMR setup consists of a GeoSpec 12 MHz low-field DRX spectrometer by Oxford Instruments, equipped with magnetic field gradients on the vertical axis. This equipment allowed monitoring of saturation profiles and produced volumes during flooding by 1D saturation profiles and 1D T_2 relaxation times distribution NMR pulse sequences, respectively. Moreover, a spatially-resolved T_2 sequence was performed for accessing longitudinal heterogeneity information, especially in the case of EST-HDT-03.

To acquire the 3D X-ray images, we used a Zeiss Xradia Versa 520 microtomograph. Energy, power and voxel size values were set to 100kV, 9W and 5µm respectively. We had a total of 3 stitches per acquisition (whole length), resulting in 30h of total acquisition time.

We used both Avizo 2020.3® and ImageJ softwares to perform 3D image processing. As presented in the protocol, we used a highly doped brine to apply differential imaging processing and segment the macropores (resolved), the matrix and the sub-resolved microporosity, defined as the pores smaller than the image resolution. This method helps us to quantify the porosity in the sub-resolved pores.

However, for flooding steps, we used B1 as formation brine. The main reason was to diminish the impact of the dopants on wettability alteration [29]. Differential imaging was no longer possible to use for saturation tracking in the sub-resolved microporosity. So we incorporate 2 different steps in the imaging protocol: total 3D images of fully oil and brine-saturated sample states.

Thus, for each different step, we normalized the 3D images (jacket and matrix) and apply a linear interpolation of the histogram peak of the sub-resolved volume, between its peaks at 100% oil and 100% brine, to average the saturation of the sub-resolved porosity. Fig. 2 helps to illustrate the image processing mentioned.

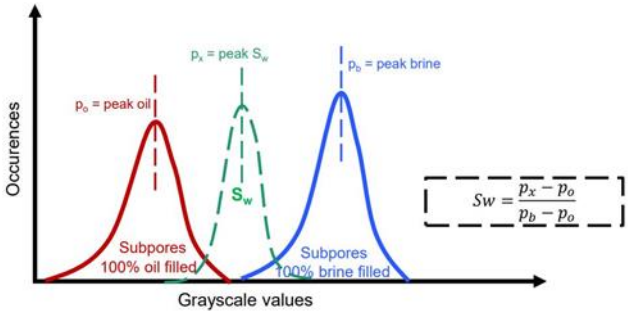

Fig. 2. Linear interpolation schematic of the histogram peak to obtain the water saturation of the sub-resolved porosity.

An important point to be highlighted is that the definition of the micro porosity term is different depending on which imaging technique was used (µ-CT or NMR):

- NMR: the definition of micro porosity (small pores) is given by a relaxation time threshold in the T_2 distribution. For Estaillades samples, signals faster than $200\,ms$ ($T_2 < 200\,ms$) are considered as microporosity. On the other hand, relaxation times slower than $200\,ms$ ($T_2 > 200\,ms$) represent the macro porosity (big pores) [30].
- µ-CT: the definition of the sub-resolved porosity by µ-CT is not based on a pore-size threshold. Therefore, as a part of the macro-porosity is sub-resolved, it is not counted as macro-porosity during differential imaging processing, thus being under-estimated.

3 Results

3.1 Viscous Oil Flood experiment

For EST-VOF-01 primary drainage experiment, we used B2 and Marcol™ 52 for the initial 5 flowrate steps. Considering that after the initial 5 steps of injection we were still far from the initial target S_{wi} of 20%, we miscibly replaced it by FINAVESTAN A 180 B for performing two oil flood steps at higher capillary number and lower flowrate. The flowrate steps used in this experiment are presented in Table 3:

Table 3 – Flowrate steps of EST-VOF-01 primary drainage

Step	Oil phase	Flowrate	Ca
1	Marcol™ 52	6 cc/h	$4.8\ 10^{-7}$
2	Marcol™ 52	60 cc/h	$4.8\ 10^{-6}$

3	Marcol™ 52	180 cc/h	1.4 10^{-5}
4	Marcol™ 52	360 cc/h	2.9 10^{-5}
5	Marcol™ 52	720 cc/h	5.7 10^{-5}
6	FINAVESTAN A 180 B	120 cc/h	5.0 10^{-5}
7	FINAVESTAN A 180 B	180 cc/h	7.5 10^{-5}

Water saturation profiles dynamics were monitored by NMR, and the profiles at the end of each flowrate step are presented in Fig. 3:

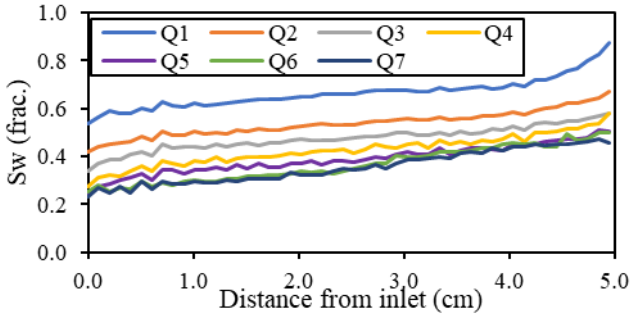

Fig. 3. Water saturation profiles during EST-VOF-01 primary drainage.

After the last step of injection, we considered that it would not be possible to reach the initial target value of S_{wi} of around 20%. Therefore, we reversed flow direction in order to homogenize the S_{wi} profile. The final profile is presented in Fig. 4, where it is possible to notice that the brine present in the initial outlet was flushed back into the sample due to the injection direction inversion. Furthermore, NMR monitoring showed that no additional brine was produced after flow reversal application (constant $S_w \approx 0.36$).

When performing the flow reversal, brine present in the initial outlet is pushed back into the sample on a water-wet imbibition process. As it is largely known, low capillary pressure regions during water-wet imbibition processes on oil/water systems exhibit hysteresis: the water phase will trap the oil phase in a snap-off mechanism. In this case, the low capillary pressure region is the initial inlet face, where oil trapping in small clusters will happen. This is an experimental artifact that may impact states restoration prior to coreflood experiments [19].

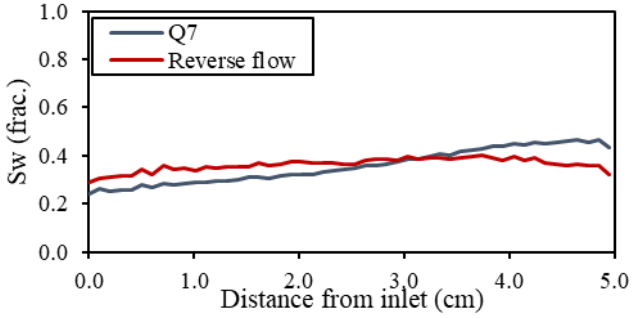

Fig. 4. S_w profiles of EST-VOF-01 prior and after injection direction inversion at the end of VOF.

3.2 HDT experiments

In order to fulfill objective (i) presented in section 1, we have performed an HDT experiment targeting a S_{wi} of around 20%. Step 1 of HDT followed two injection flowrate steps using Marcol™ 52 (30 cc/h and 60 cc/h). We monitored saturation change using a graduated burette connected to the outlet tubing of our sample. As both the oil and the brine phases produce NMR signal, it is not possible to perform a saturation profile monitoring during drainage by Spin-Echo Single-Point Image (SE-SPI) sequences. The solution for undistinguished visualization of both phases by NMR and to obtain a saturation profile during primary drainage was to miscibly replace Marcol™ 52 by toluene. As toluene is around 21 times less viscous than Marcol™ 52, it has a much longer relaxation time distribution, which enables a separation of its signal from the brine in the T_2 relaxation times distribution, as verified in Fig. 5. By performing a spatially-resolved T_2 measurement, we were able to obtain the saturation profile curves at the end of each HDT Step.

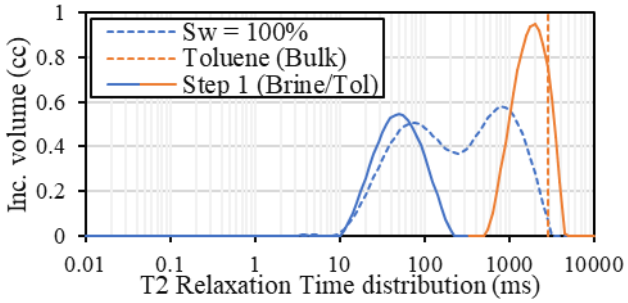

Fig. 5. T_2 Relaxation Times distribution after Step 1 of HDT (EST-HDT-01). A clear separation of the toluene and brine signals is possible in the T2 relaxation times distribution.

Moving on to the Step 2 of HDT, we applied $P_c = 5\ bar$ following the trend of the $P_c\ vs.\ S_w$ curve of an Estaillades limestone sample presented in [31]. According to the author, this P_c would take the sample to an S_{wi} value of around 20%.

A T_2 relaxation time distribution measurement performed at the end of Step 2 of HDT indicates that water present as the wetting phase in the small pores has been expelled by the oil (non-wetting phase), as the brine signal reduces in amplitude and moves slightly towards the left (lower relaxation times – increasing its surface relaxation). Simultaneously, it is possible to observe an increase in magnitude of the toluene signal, with no horizontal shift. This indicates that the toluene is non-wetting, as it relaxes at its bulk relaxation time [32]. This observation may be seen in Fig. 6. The final S_w profiles obtained after the treatment of the spatially-resolved T_2 measurements at the end of Steps 1 and 2 of HDT are presented in Fig. 7.

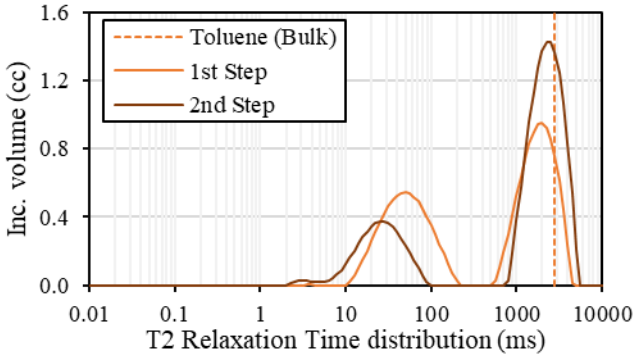

Fig. 6. T_2 Relaxation Times distribution comparison between the end of Steps 1 and 2 (EST-HDT-01).

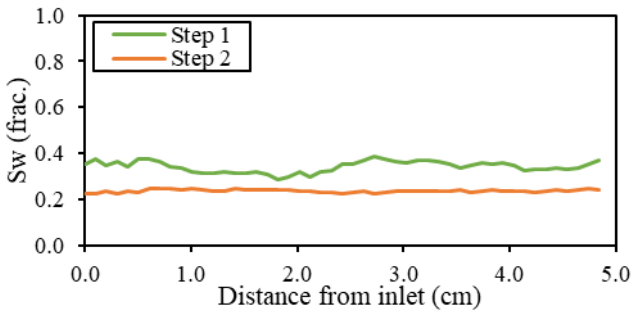

Fig. 7. EST-HDT-01 saturation profiles at the end of both Steps of HDT.

It is interesting to observe that, even though the profile at the end of Step 1 was obtained at the end of a VOF displacement, there is no detection of CEE. This is probably explained by a profile equilibration, as the delay between the end of Step 1 and the Spatially-resolved T_2 acquisition for the definition of the S_w profile was consequent.

As the results of the NMR measurements and the material balance (graduated burette) agreed, we may confirm that the target value of S_{wi} ($S_{wi,target} \approx 0.20$) was achieved. This is an important result in the evaluation of VOF and HDT application on bimodal limestone samples. It proves HDT ability to desaturate a core sample to a low S_{wi} value without imposing high Capillary Number floods that could cause sample damage and fines migration.

After this initial validation, EST-HDT-02 and EST-HD-03 samples were used to fulfill the objective (ii) presented in section 1. For that, both samples were drained to the same level of S_{wi} as EST-VOF-01 ($S_{wi} \approx 0.38$) by HDT. The homogeneous profile produced during EST-HDT-02 primary drainage is presented in Fig. 8:

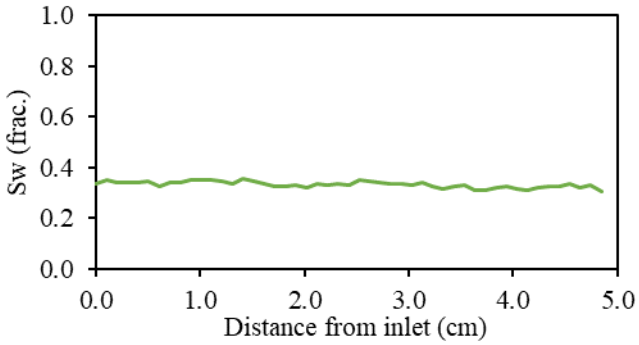

Fig. 8. S_{wi} profile of EST-HDT-02, obtained by an NMR SE-SPI sequence.

Regarding sample EST-HDT-03, an initial characterization by NMR and µ-CT allowed interesting observations, as porosity homogeneity is investigated both in the pore (µ-CT) and the core-scale (NMR). The total porosity profiles are presented in Fig. 9. It is interesting to observe that a very similar result was obtained using two completely different tools, at two different scales of observation.

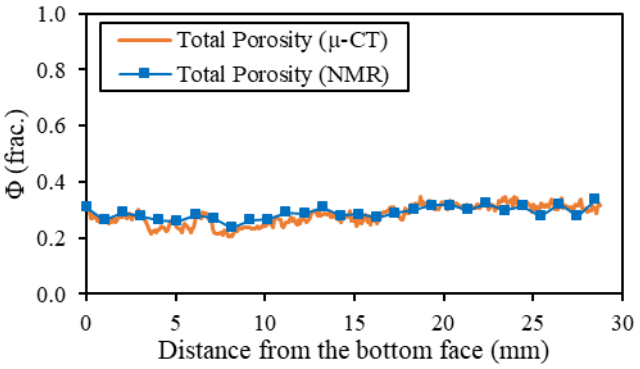

Fig. 9. Total porosity longitudinal profiles by NMR and µ-CT analysis.

Furthermore, Estaillades limestone samples are known for their bimodal porosity characteristics. To investigate the distribution of micro and macro pores, we performed spatially-resolved T_2 for NMR analysis of the porosity and differential imaging for µ-CT investigation. We present, in Fig. 10 and Fig. 11, the direct comparison between the macro and micro-porosity curves obtained by NMR and µ-CT. It is possible to verify the coherence between the results and the definition about the threshold defining big and small pores according to the used imaging tool provided in sub-section 2.3.

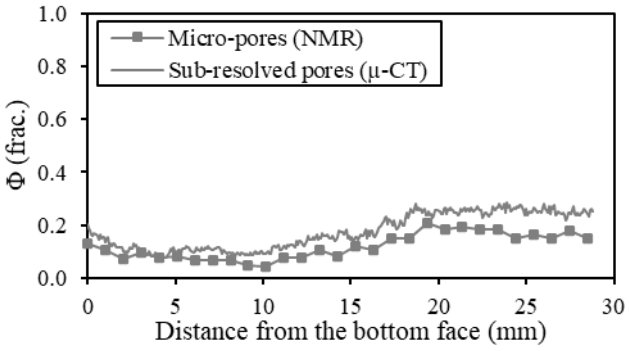

Fig. 10. Micro-pores distribution according to NMR (spatially-resolved T2) and µ-CT (differential imaging).

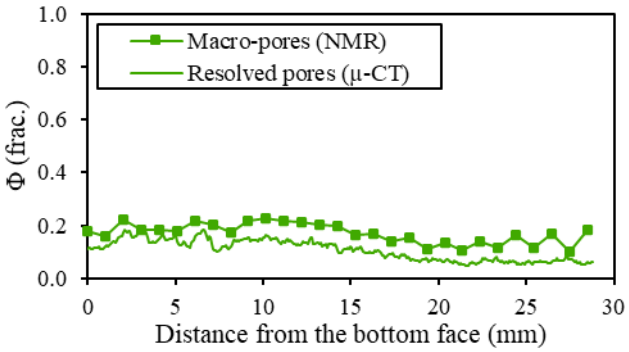

Fig. 11. Macro-pores distribution according to NMR (spatially-resolved T2) and µ-CT (resolved pores - differential imaging).

The protocol presented at the beginning of section 2.2 was used for the primary drainage of samples EST-HDT-02 and EST-HDT-03, except for the capillary pressure imposed during Step 2 of HDT. In the case of these samples, the applied P_c is equal to 1 bar, as the target value of S_{wi} was approximately 0.38.

It is difficult to conclude on the effects of HDT over the unresolved porosity, due to along axis heterogeneity. For a better understanding of the phenomenology in the sub-resolved porosity of EST-HDT-03 during HDT and to remove the effect of heterogeneities in the analysis, we normalized water saturation in Steps 1 and 2 using equation (1), as presented below:

$$\|S_{w\,sub}(x)\| = \frac{V_{w\,sub}(x)}{\varphi_{sub}(x)} \quad (1)$$

where $\|S_{w\,sub}(x)\|$ is the normalized water saturation in the sub-resolved porosity at a position x in the sample, $V_{w\,sub}(x)$ is the water volume in the sub-resolved porosity at the position x, and $\varphi_{sub}(x)$ is the sub-resolved porosity in position (x). The same approach was applied for the resolved porosity.

This approach allows the elimination of porosity heterogeneity effects on the profiles. Therefore, we were able to analyze the saturation profiles behaviour in both porosities separately. The water saturation profiles obtained by µ-CT analysis (differential imaging) for both porosities at the end of Steps 1 and 2, using the above described protocol, are presented in Fig. 12 and Fig. 13:

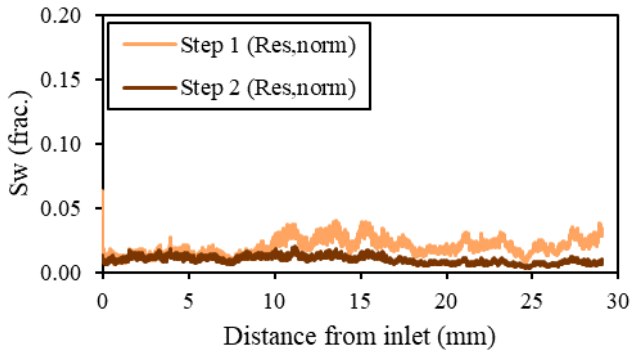

Fig. 12. Normalized water saturation profiles of the resolved porosity at the end of Steps 1 and 2.

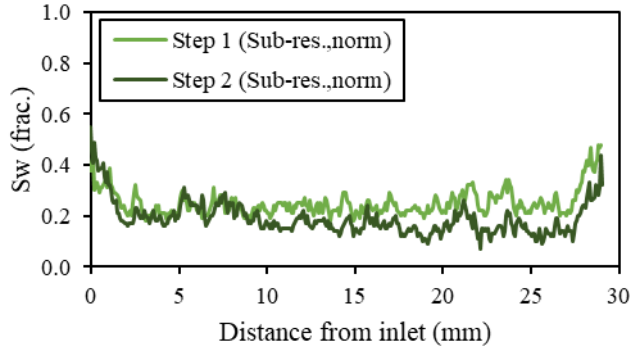

Fig. 13. Normalized water saturation profiles of the micro (sub-resolved) porosity at the end of Steps 1 and 2.

The curves evolution presented here above are an important indication that HDT is effective on accessing smaller porosity by imposing a homogeneous capillary pressure field in the core sample. Moreover, by performing the normalization of the saturation, we are able to identify the elimination of the CEE at the end of Step 2 of HDT.

3.3 Waterflooding experiments

In order to perform a clear comparison of the waterflooding results, we used roughly the same protocol during imbibition for samples EST-VOF-01 and EST-HDT-02, apart from the initial injection flowrate step (Q1). The applied flowrates and the associated Capillary Numbers are presented in Table 4:

Table 4 – Flowrate steps and associated Capillary Numbers for EST-VOF-01 and EST-HDT-02 waterflooding.

Step	Flowrate	Ca	Step	Flowrate	Ca
Q1*	3 cc/h	$2.6\ 10^{-8}$	Q5	48 cc/h	$4.2\ 10^{-7}$
Q2	6 cc/h	$5.2\ 10^{-8}$	Q6	96 cc/h	$8.4\ 10^{-7}$
Q3	12 cc/h	$1.0\ 10^{-7}$	Q7	192 cc/h	$1.7\ 10^{-6}$
Q4	24 cc/h	$2.1\ 10^{-7}$			

*Q1 was used only on EST-HDT-02 waterflooding

3.4 Numerical Simulation

A Darcy-scale numerical simulation of the imbibition relative permeability and capillary pressure for EST-VOF-01 and EST-HDT-02 was performed using CYDAR®; a numerical simulator for design and interpretation of petrophysical laboratory experiments.

In the numerical simulation, we matched the pressure drop between sample inlet and outlet (dP), the produced oil volumes (V_o) and the water saturation profiles during waterflooding. We used the Corey model [33] as the analytical function for the definition of EST-VOF-01 K_r. Corey expressions are useful for describing the relative permeability behaviour between residual end points based on normalized phase saturation. In the case of imbibition, the normalized oil and water relative permeabilities are defined by equations (2) and (3):

$$k_{ron} = S_{on}^{\ No} \quad (2)$$

$$k_{rwn} = S_{wn}^{\ Nw} \quad (3)$$

where S_{on} and S_{wn} are the normalized oil and water saturations, given by (4) and (5):

$$S_{on} = \frac{1 - S_w - S_{or}}{1 - S_{wi} - S_{or}} \quad (4)$$

$$S_{wn} = \frac{S_w - S_{wi}}{1 - S_{wi} - S_{or}} \quad (5)$$

When experimental artifacts are prevented, N_o and N_w exponents carry important information regarding the rock's wettability, as they define the dynamic behaviour of fluids flow.

For the capillary pressure curve, we used the LogBeta function [34]. This is an analytical function used to define the shape of the $P_c(S_w)$ curve based on the experimental data.

The general P_c LogBeta function, with no threshold, is defined as:

$$P_c = -\frac{A}{\beta} P_0 \left(\ln \frac{S^{*\beta}}{1 - S^{*\beta}} - \ln \frac{(1 - S^*)^\beta}{1 - (1 - S^*)^\beta} \right) + b \quad (6)$$

The magnitude P_0 and the saturation S_0 (water saturation at $P_C = 0$) are "physical parameters", and they are related to factor "b" by:

$$b = \frac{A}{\beta} P_0 \left(\ln \frac{S^{*\beta}_0}{1 - S^{*\beta}_0} - \ln \frac{(1 - S^*_0)^\beta}{1 - (1 - S^*_0)^\beta} \right) \quad (7)$$

The parameter "A" is calculated for the continuity of the curve.

For the imbibition case, the pressure threshold is typically applied at the minimum normalized saturation value $S^* = 0$, and P_c, for S^* values greater than the threshold, are defined according to the equation presented here below:

$$P_c < P_t \rightarrow P_c = -P_0 \frac{1}{(1 - S^*)} \qquad (8)$$

The resulting imbibition K_r, P_c and saturation profiles from the waterflooding history-match are presented in Fig. 14, Fig. 15 and Fig. 16. The used parameters for the deconvolution are presented in Table 5.

The negative P_t parameter in both cases means that no spontaneous imbibition is expected, as a negative capillary pressure is necessary to change saturation.

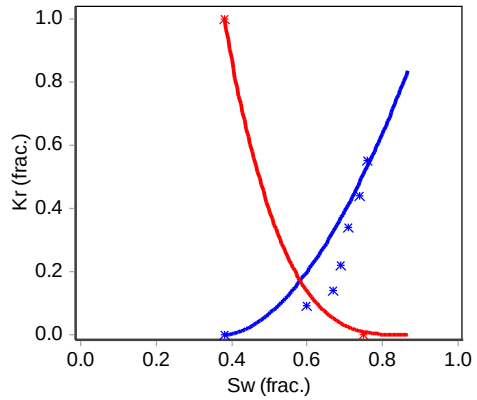

Fig. 14. K_r imbibition curve (EST-VOF-01). The blue stars represent the experimentally measured water relative permeability.

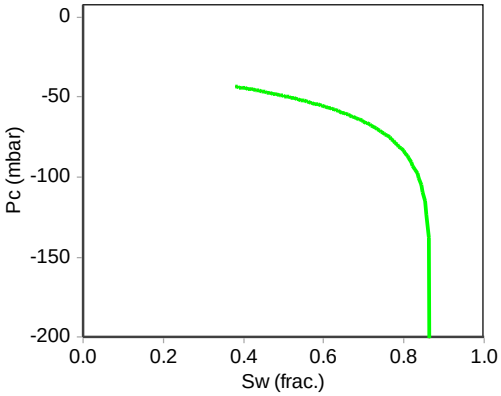

Fig. 15. P_c imbibition curve of EST-VOF-01.

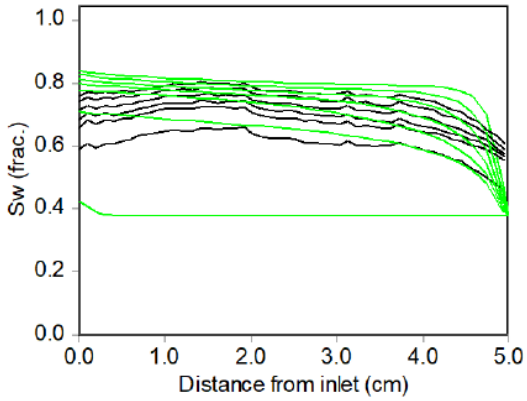

Fig. 16. History-match of S_w profiles during EST-VOF-01 waterflooding.

Table 5 - Set of parameters used for EST-VOF-01 imbibition K_r and P_c history match.

Basic properties	D (cm)	3.78
	L (cm)	5.00
	$K_{base} = K_{o@Swi,AA}$ (mD)	160
	Φ (frac.)	0.305
K_r (Corey)	K_{rw} max (frac.)	0.84
	K_{ro} max (frac.)	1.00
	S_{wi} (frac.)	0.38
	$S_w(S_{or})$ (frac.)	0.87
	N_w (dim.)	1.8
	N_o (dim.)	3.3
P_c (LogBeta)	P_0 (mbar)	20.56
	$P_{threshold}$ (mbar)	-43.29

In the case of EST-HDT-02, we used the LET model for relative permeability [35]. This function allows a better representation of a potential sigmoidal and/or heterogeneous behavior of the relative permeability, which is not captured by the Corey model. For an oil-water system, the model is given by (9) and (10):

$$k_{row} = k_{row,max} \frac{(1 - S_{wn})^L}{(1 - S_{wn})^L + E \cdot (S_{wn})^T} \qquad (9)$$

$$k_{rw} = k_{rw,max} \frac{(S_{wn})^L}{(S_{wn})^L + E \cdot (1 - S_{wn})^T} \qquad (10)$$

As previously presented for EST-VOF-01, K_r, P_c and S_w profiles obtained after the waterflooding history-match of EST-HDT-02 are presented in Fig. 17 and Fig. 18. The used parameters for the deconvolution are presented in Table 6.

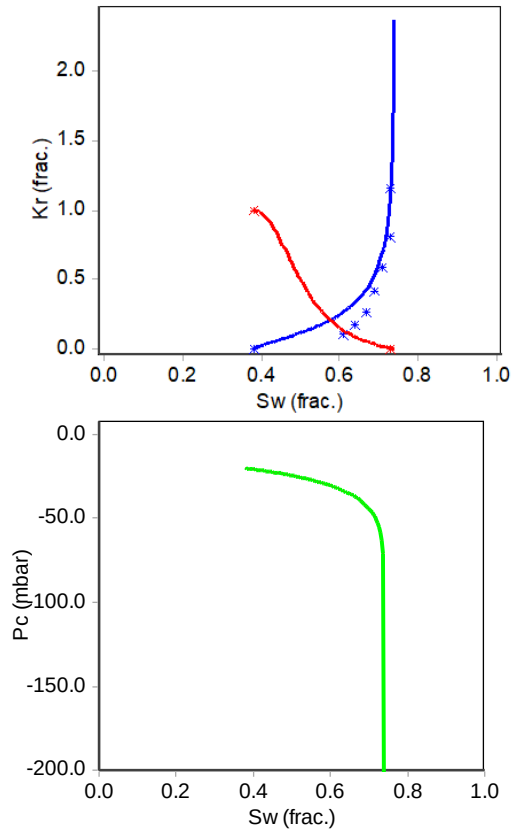

Fig. 17. K_r and P_c imbibition curves of EST-HDT-02

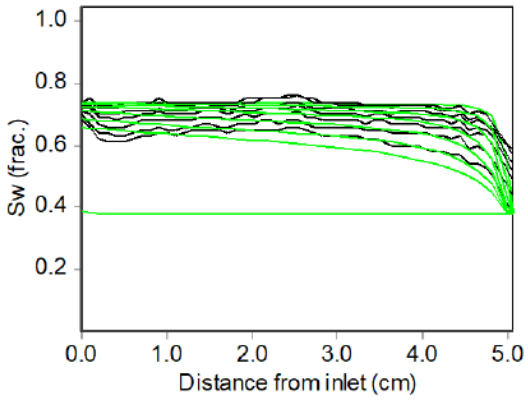

Fig. 18. History-match of S_w profiles during EST-HDT-02 waterflooding.

Table 6 - Set of parameters used for EST-HDT-02 imbibition K_r and P_c history match.

Basic properties	D (cm)		3.79	
	L (cm)		5.07	
	$K_{base} = K_{o@Swi,AA}$ (mD)		106	
	Φ (frac.)		0.316	
K_r (LET)	K_{rw} max (frac.)		2.4	
	K_{ro} max (frac.)		1.0	
	S_{wi} (frac.)		0.38	
	$S_w(S_{or})$ (frac.)		0.74	
	Water		**Oil**	
	L	0.78	L	0.93
	E	10.73	E	6.20
	T	0.64	T	2.00
P_c (LogBeta)	P_0 (mbar)		11.00	
	$P_{threshold}$ (mbar)		-20.00	

When comparing the relative permeability curves obtained after history match, we face some interesting findings. For a clear comparison of the behavior of the samples relative permeability during imbibition, we present the curves in both linear and semi-log scale in Fig. 19 and Fig. 20.

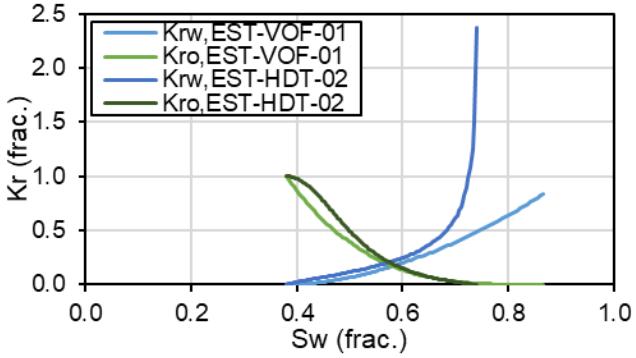

Fig. 19. Imbibition K_r curves in linear and semi-log scale for EST-VOF-01 (lighter colors) and EST-HDT-02 (darker colors).

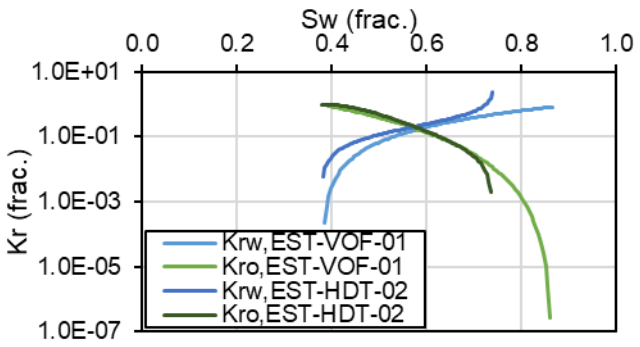

Fig. 20. Imbibition K_r curves in linear and semi-log scale for EST-VOF-01 (lighter colors) and EST-HDT-02 (darker colors).

4 Discussion

4.1 Kr expression used for the history match and lower Sw range behavior

Performing the history match using Corey expressions is only possible for EST-VOF-01. This result is important, because the Corey approach assumes a monomodal, homogeneous core, which K_r follows a power trend. Considering that the Estaillades is a bimodal sample and flow is controlled by the big pores, this result confirms that, during primary drainage by VOF, virtually no oil was flushed in the small pores.

This is not the case for EST-HDT-02. For this sample, acceptable waterflooding history match for relative permeability curves definition is only possible using the LET expression, suited for matching samples that does not follow a power behavior. In the case of EST-HDT-02, oil entered the small pores during primary drainage due to the filling process of Step 2 (capillary-controlled). This assumption is supported by a µ-CT scan of sample EST-HDT-03 performed at the end of primary drainage, which followed the same experimental protocol as EST-HDT-02 in terms of capillary number during Step 1 and capillary pressure in Step 2.

Considering these indications, first oil production during EST-HDT-02 waterflooding occurs by capillarity of the smaller pores, as brine slowly invades the sample during the first flowrate step. As oil relative permeability is controlled by the bigger pores and smaller pores has minor impact in the general oil mobility, we notice a slow decrease in oil relative permeability for the lower range of water saturation in the case of EST-HDT-02 ($S_{wi} \approx 0.38 \leq S_w \leq 0.50$). From this point on, oil production will continue by displacement of oil present in the bigger pores, where a faster decrease in oil relative permeability is observed.

Regarding the behavior of water relative permeability curves in the lower range of water saturation, a difference between the curves is only noticeable in the semi-log plot. It is possible to observe that $K_{rw}(VOF)$ increases sharply, whereas $K_{rw}(HDT)$ has a slower increase. This result is coherent with the interpretation presented in the previous paragraphs. For VOF, as water replaces oil present in the bigger pores, it significantly increases its mobility. In the case of HDT, a slow increase in K_{rw} is related to an initial production of oil present in the smaller pores, which have a minor impact in water relative permeability. The hypotheses assumed before water breakthrough are based on the analysis of the µ-CT scan of the sub-resolved porosity of EST-HDT-03 at the end of waterflooding, presented in Fig. 22.

4.2 Sor ranges

One important parameter when analyzing imbibition relative permeability curves regarding wettability is the S_{or}. At a first look, we would be tempted to state that only EST-VOF-01 behaves as an oil-wet sample and the behavior of EST-HDT-02 would be rather related to a water-wet rock, given both samples S_{or} [25]. However, in the case of Estaillades, S_{or} analysis may hide some aspects regarding the total volume of trapped oil after waterflooding, usually considered when analyzing a sample wettability during waterflooding (snap-off trapping during waterflooding). Considering that Estaillades are dual-porosity rocks, we should consider the presence of oil in both big and small pores, especially for sample initialized by the HDT, where we have indications that oil invaded the small pores during primary drainage.

The waterflooding is a viscous-controlled process such as the Viscous Oil Flood, meaning that the same constraints regarding small pores by-passing will be valid to this process. Then, if a sample presents oil in both big and small pores, it is logical to state that oil will be trapped in smaller pores by the doublet mechanism. Hence, even though a high value of S_{or} (usually related to water-wet cores) is observed for EST-HDT-02, it can still behave as mixed or oil-wet.

Given these considerations, we may interpret the high S_{or} value obtained for EST-HDT-02 as oil trapping in smaller pores. As we have seen from the NMR results after primary drainage, oil invaded small pores during Step 2 of HDT. Moreover, EST-HDT-03 provided a pore-scale visualization of the Hybrid Drainage process, which validated oil phase invasion in smaller pores. On the other hand, as Viscous Oil Flood primary drainage does not allow oil to invade smaller pores homogeneously, the sample behavior during waterflooding is governed mostly by the bigger pores, hence as a monomodal porosity sample. It makes sense to observe a lower S_{or} value in this case, as there is much less oil trapping in smaller pores due to the doublet mechanism. We present in Fig. 21 two slices of EST-HDT-03 at the end of waterflooding where it is possible to notice oil presence in the smaller pores of the sample, corroborating the analysis described here above.

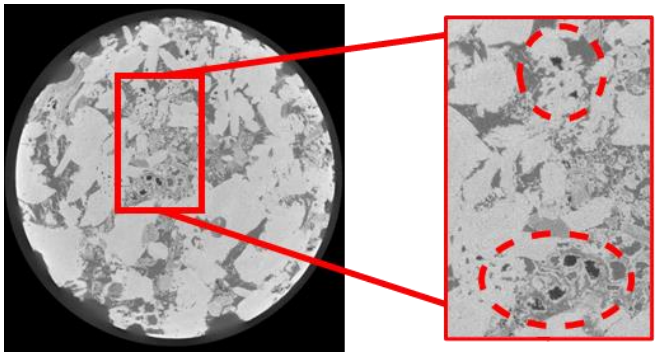

Fig. 21. EST-HDT-03 after waterflooding. The red circles highlight oil trapping in the smaller pores.

Considering the K_r curves for EST-HDT-02 and EST-VOF-01 presented in Fig. 19 and Fig. 20, we notice that the behavior during waterflooding is quite similar for a wide range of S_w ($0.50 \leq S_w \leq 0.70$). The K_r ratio between the history-matched relative permeabilities are different in the range close to S_{wi}, because of the reasons evoked in the preceding sub-section, and differ once again for values close to S_{or}, which corroborates the analysis of oil trapping in the smaller pores at the end of waterflooding.

Moreover, by performing differential imaging treatment, we are able to identify the brine presence in both resolved and sub-resolved porosities separately (after ageing and at ROS), as presented in Fig. 22. A normalization of the saturation profile of both small and big pores saturations was done, as previously discussed.

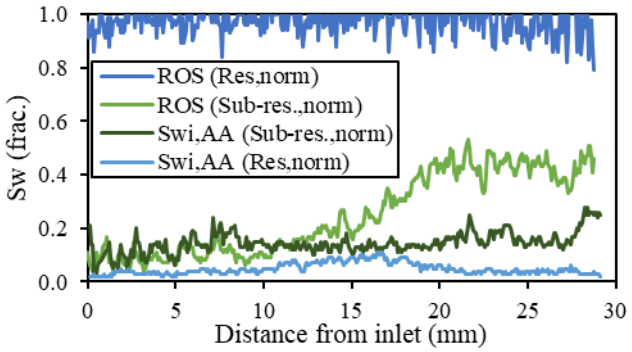

Fig. 22. Normalized S_w profiles of resolved and sub-resolved pores after ageing and after waterflooding (ROS) (EST-HDT-03).

Regarding the resolved-porosity saturation profiles, it is possible to notice that a recovery value close to unity was obtained, departing from a very low initial water saturation after ageing. This is possibly due to a film recovery mechanism [18], which would represent a mixed-wet behavior of this fraction of the sample. The remaining oil present in this region is held back in the form of thin films, that are difficult to detect by µ-CT imaging.

On the other hand, analyzing the small pores saturation profiles between the end of the ageing and waterflooding steps, supports the hypothesis of early oil production by capillarity invasion and further oil trapping at the end of waterflooding. Considering that this network was poorly flushed by crude oil during ageing due to the pore network configuration of the Estaillades samples, it is logical to presume that wettability alteration was less pronounced than in the bigger porosity network. Therefore, early production by capillarity through water-wet thin pores networks would explain the observed evolution of the S_w profile between S_{wi} and ROS states. This evolution indicates that oil production is not due to the application of viscous forces, given that brine accumulates close to the outlet face during waterflooding (where there is a bigger presence of small pores). Furthermore, it is clearly visible that the Remaining Oil Saturation (ROS) at the end of waterflooding is trapped in the small-pore network, which supports the hypothesis enounced in this section.

4.3 Krw behavior close to Sor

Another indication of oil trapping in the smaller porosity for EST-HDT-02 and EST-HDT-03 is K_{rw} behavior close to S_{or}. It is clearly noticeable that water relative permeability increases sharply until a $K_{rw}(S_{or})$ value close to the initial K_w value, despite a high S_{or} value. This behavior of the K_r curve indicates that brine flows at the center of the bigger pores at almost the same mobility as in a monophasic flow, despite the presence of residual oil. This effect may be related to what is sometimes observed on water-wet samples at the end of primary drainage ($K_{ro}(S_{wi}) > K_w$) [36].

5 Conclusions and perspectives

5.1 VOF

Most currently used technique for setting S_{wi} value in full-size cores during SCAL routines, the VOF presents the main disadvantage of generating CEE during primary drainage in water-wet samples. We tested the solution of reversing injection direction for the reduction of Capillary-End Effects, which has proven to be efficient, macroscopically, albeit hysteresis effects. However, we showed, by NMR imaging, that this approach mobilizes brine present in the sample outlet, which is re-injected following an imbibition process. It has been recently reported that this phenomenon may, indeed, impact states initialization, due to saturation hysteresis [19].

In addition, being a viscous-controlled method, VOF is not suited for the desaturation of dual-porosity samples for low targets of S_{wi}. During this project we tested the method on an Estaillades sample and reaching values of S_w below 35% has proven to be impossible.

5.2 HDT

This method proved, once again, to be efficient on eliminating CEE and generating a homogeneous saturation profile at the end of primary drainage. We verified the homogeneity of the produced saturation profiles by NMR and µ-CT imaging, as well as pore occupancy change (µ-CT) between Steps 1 and 2, which showed the desaturation of zones not invaded by oil during the viscous-based displacement during Step 1.

Notwithstanding, it was effective on desaturating bimodal limestone samples at low target S_{wi} values, as seen on the results of the EST-HDT-01 sample.

5.3 Waterflooding comparison

We compared the waterflooding history match of Estaillades samples initiated by two different primary drainage techniques (Viscous Oil Flood and Hybrid Drainage Technique). The difference between the resulting imbibition K_r and P_c curves are related, mostly, to the ability of the techniques to invade both bigger and smaller pores of the sample during the primary drainage step.

As HDT experiments are able to invade smaller pores during primary drainage, they present higher K_{rw} as there is oil trapping in smaller pores by the doublet mechanism. In addition, difference in K_{rw} behavior close to S_{wi} and S_{or} may also be explained by the difference in pore occupancy after primary drainage. These assumptions and hypotheses are based on the history match results and the pore-scale visualization by µ-CT.

The resulting history matched K_r and P_c curves are used to feed numerical simulations to provide production profile in reservoir engineering. As these are among the most relevant parameters in waterflooding experiments on core samples analysis, the importance of using a primary drainage method representative of the reservoir behavior is quite clear, proving all the value of the Hybrid Drainage Technique.

6 Nomenclature

Abbreviations

CCA	Conventional Core Analysis
CEE	Capillary-End Effects
EST	Estaillades limestone
HDT	Hybrid Drainage Technique
$MICP$	Mercury Injection Capillary Pressure
NMR	Nuclear Magnetic Resonance
PD	Primary Drainage
ROS	Experimentally-obtained Remaining Oil Saturation
$SCAL$	Special Core Analysis
VOF	Viscous Oil Flood

Symbols

K_r	Relative Permeability
K_{eff}	Effective Permeability
$K_{r"i"n}$	Phase "i" normalized relative permeability
$K_{rw}(SOR)$	Water relative permeability at Residual Oil Saturation
N_o	Corey exponent to oil
N_w	Corey exponent to water
P_c	Capillary Pressure
P_0	Capillary pressure magnitude in the LogBeta function
P_t	Capillary pressure threshold in the LogBeta function
S^*	Normalized fluid saturation
$S_{"i"}$	Phase "i" saturation
S_{or}	Residual Oil Saturation
S_{wi}	Initial Water Saturation
$\|S_{w_{sub}}(x)\|$	Normalized water saturation (sub-resolved porosity) in position x
V_o	Oil Volume
V_p	Pore Volume
$V_{w_{sub}}(x)$	Water volume (sub-resolved porosity) in position x

7 References

1. V. Fernandes, C. Caubit, B. Nicot, F. Pairoys, H. Bertin, J. Lachaud, Petrophysics, *Hybrid Technique for setting initial water saturation on core samples* **64 (03),** 325-339. (2023)
2. T. Vandamme, E. Caroli, S. Gratton, Petrophysics, *How the Invasion Zone Can Contribute to the Estimation of Petrophysical Properties From Log Inversion at Well Scale?*, **60 (02)**, 306-325. (2019)
3. F. Kuchuk, L. Zhan, S. M. Ma, A. M. Al-Shahri, T.S. Ramakrishnan, Y. B. Altundas, M. Zybek, R. de Loubens, N. Chugnov, SPE Reservoir Evaluation & Engineering, *Determination of In Situ Two-Phase Flow Properties Through Downhole Fluid Movement Monitoring*, 13 (04), 575-587. (2010)
4. L. Liang; L. Venkataramanan, S. Wang, F. C. Canesin, V. M. Gkortsas, K. Cig, A. Abubakar, T. M. Habashy, SPWLA 59th Annual Logging Symposium, *Estimating in-situ relative permeability and capillary pressure from multiphysics wireline measurements*, (2018)
5. S. M. Ma, M. Amabeoku, Interpretation, *Core analysis with emphasis on carbonate rocks—quality assurance and control for accuracy and representativeness*, **3 (1)**. (2015)
6. C. McPhee, J. Reed, I. Zubizarreta, *Core analysis: a best practice guide*. Elsevier (2015)
7. G. Singer, W. Shao, S. Chen, P. Hawley, Z. H. Xie, S. M. Ma, SPWLA 63rd Annual Logging Symposium, *Evaluating the Effectiveness of Rock Cleaning*. (2022)

8. D. Tiab, E. C. Donaldson, *Petrophysics: theory and practice of measuring reservoir rock and fluid transport properties*. Gulf professional publishing. (2015)
9. A. Al-Harbi, D. P. Schmitt, S. M. Ma, SPE Annual Technical Conference and Exhibition, *Toward quantitative remaining oil saturation (ROS): determination challenges and techniques*, (2011)
10. D. Jia, J. S. Buckley, N. R. Morrow, SPE International Symposium on Oilfield Chemistry. *Control of core wettability with crude oil*. (1991)
11. P. P. Jadhunandan, N. R. Morrow, In Situ, *Spontaneous imbibition of water by crude oil/brine/rock systems*., **15**. (1991)
12. P. Zhang, T. Austad, SPE Europec/EAGE Annual Conference, *Waterflooding in Chalk: Relationship between Oil Recovery, New Wettability Index, Brine Composition and Cationic Wettability Modifier*. (2005)
13. M. C. Leverett, W. B. Lewis, Transactions of the AIME, *Steady flow of gas-oil-water mixtures through unconsolidated sands*, 107-116. (1941)
14. J. M. Lombard, S. Gautier, P. Egermann, O. Vizika, E. Tachet, SCA, *Petrophysical Parameter Measurements: Comparison.* (2006)
15. A. Graue, E. Aspenes, T. Bognø, R. W. Moe, J. Ramsdal, Journal of Petroleum Science and Engineering, *Alteration of wettability and wettability heterogeneity,* **33**, 3-17. (2002)
16. E. Johannesen, J. Howard, A. Graue, SCA, *Evaluation of wettability distributions in experimentally aged core.* (2008)
17. M. Mascle, S. Youssef, H. Deschamps, O. Vizika, Petrophysics, *In-situ investigation of aging protocol effect on relative permeability measurements using high-throughput experimentation methods,* **60**, 514-524. (2019)
18. R. A. Salathiel, JPT, *Oil recovery by surface film drainage in mixed-wettability rocks*, 1216-1224. (1973)
19. F. Nono, C. Caubit, R. Rivenq, SCA, *Initial states of coreflooding techniques evaluation: a global pore-scale investigation*, (2022).
20. F. Nono, PhD Thesis, *Caractérisation polyphasique de la zone de transition dans un réservoir pétrolier carbonaté,* Ecole Nationale Supérieure d'Arts et Métiers. (2014)
21. H. Ott, C. H. Pentland, S. Oedai, International Journal of Greenhouse Gas Control, *CO2–brine displacement in heterogeneous carbonates*, **33**, 135-144. (2015)
22. Y. Gao, A. Q. Raeini, , M. J. Blunt, B. Bijeljic, Advances in Water Resources, *Pore occupancy, relative permeability and flow intermittency measurements using X-ray micro-tomography in a complex carbonate,* **129**, 56-59. (2019)
23. Q. Lin, B. Bijeljic, S. Foroughi, S. Berg, M. J. Blunt, Chemical Engineering Science, *Pore-scale imaging of displacement patterns in an altered-wettability carbonate*, **235**. (2021)
24. M. Fleury, Y. Santerre, B. Vincent, SPWLA 48th Annual Logging Symposium, *Carbonate rock typing from NMR relaxation measurements*. (2007)
25. M. J. Blunt, *Multiphase flow in permeable media: A pore-scale perspective*, Cambridge University press. (2017)
26. N. R. Morrow, H. T. Lin, J. S. Ward, SPE Formation Evaluation, *Effect of crude-oil-induced wettability changes on oil recovery,* **1**, 89-103. (1986)
27. A. Graue, ,B. G. Viksund, B. A. Baldwin, SPE Reservoir Evaluation & Engineering, *Reproducible wettability alteration of low-permeable outcrop chalk*, **2 (02)**, 134-140. (1999)
28. Q. Lin, Y. Al-Khulaifi, M. J. Blunt, B. Bijeljic, Advances in water resources, *Quantification of sub-resolution porosity in carbonate rocks by applying high-salinity contrast brine using X-ray microtomography differential imaging,* **96**, 306-322. (2016)
29. F. Pairoys, C. Caubit, F. Nono, L. Rochereau, A. Nepesov, Q. Danielczick, N. Agenet, SCA, *Impact of dopants on SCAL experiments, phase I.* (2023 – To be published)
30. M. Fleury, Y. Santerre, B. Vincent, SPWLA 48th Annual Logging Symposium, *Carbonate rock typing from NMR relaxation measurements.* (2007)
31. V. Fernandes, PhD Thesis, *Experimental study of fluid setting in natural porous media: Application to reservoir rocks,* Université de Bordeaux. (2023)
32. A. Valori, B. Nicot, Petrophysics, *Review of 60 years of NMR wettability,* **60 (02)**, 255-263. (2019)
33. A. T. Corey, C. H. Rathjens, J. H. Henderson, M. R. Wyllie, Journal of Petroleum Technology, *Three-phase relative permeability*, **8 (11)**, 63-65. (1956)
34. CYDAREX, *CYDAR-SCAL User Manual*. (2021)
35. F. Lomeland, E. Ebeltoft, W. H. Thomas, SCA, *A new versatile relative permeability correlation*. (2005)
36. S. Berg, A. W. Cense, J. P. Hofman, R. M. M. Smits, SCA, *Flow in porous media with slip boundary condition.* (2007)